

Article

Shape-Memory Nanofiber Meshes with Programmable Cell Orientation

Eri Niiyama ^{1,2}, Kanta Tanabe ^{1,3}, Koichiro Uto ⁴, Akihiko Kikuchi ⁵ and Mitsuhiro Ebara ^{1,2,3,*} 

¹ International Center for Materials Nanoarchitectonics (WPI-MANA), National Institute for Materials Science (NIMS), Tsukuba, Ibaraki 305-0044, Japan; s1630131@u.tsukuba.ac.jp (E.N.); tanabe19331510@yahoo.co.jp (K.T.)

² Graduate School of Pure and Applied Sciences, University of Tsukuba, Tsukuba, Ibaraki 305-8577, Japan

³ Graduate School of Industrial Science and Technology, Tokyo University of Science, Katsushika, Tokyo 125-8585, Japan

⁴ International Center for Young Scientists (ICYS), National Institute for Materials Science (NIMS), Tsukuba, Ibaraki 305-0044, Japan; uto.koichiro@nims.go.jp

⁵ Department of Materials Science and Technology, Tokyo University of Science, Katsushika, Tokyo 125-8585, Japan; kikuchia@rs.noda.tus.ac.jp

* Correspondence: ebara.mitsuhiro@nims.go.jp

Received: 14 February 2019; Accepted: 25 February 2019; Published: 1 March 2019



Abstract: In this work we report the rational design of temperature-responsive nanofiber meshes with shape-memory properties. Meshes were fabricated by electrospinning poly(ϵ -caprolactone) (PCL)-based polyurethane with varying ratios of soft (PCL diol) and hard [hexamethylene diisocyanate (HDI)/1,4-butanediol (BD)] segments. By altering the PCL diol:HDI:BD molar ratio both shape-memory properties and mechanical properties could be readily turned and modulated. Though mechanical properties improved by increasing the hard to soft segment ratio, optimal shape-memory properties were obtained using a PCL/HDI/BD molar ratio of 1:4:3. Microscopically, the original nanofibrous structure could be deformed into and maintained in a temporary shape and later recover its original structure upon reheating. Even when deformed by 400%, a recovery rate of >89% was observed. Implementation of these shape memory nanofiber meshes as cell culture platforms revealed the unique ability to alter human mesenchymal stem cell alignment and orientation. Due to their biocompatible nature, temperature-responsivity, and ability to control cell alignment, we believe that these meshes may demonstrate great promise as biomedical applications.

Keywords: shape memory nanofiber; shape memory polymer; poly(ϵ -caprolactone); melting temperature; cell orientation; polyurethane

1. Introduction

Stimuli-responsive fibrous materials with shape-memory properties (also called “shape-memory fibers”) have received great attention for their potential regenerative medicine, filtration, robotics, and catalysis applications [1–8]. Shape-memory polymers (SMPs) are a class of temperature-responsive materials that can change from a temporary shape to a memorized permanent shape upon the application of heat. Both glass transition temperature (T_g) and melting temperature (T_m) have been leveraged to initiate shape-switching; however, T_m is often favored in the design of SMPs because the enthalpy changes of the solid–liquid phase transition are much larger than that of the glass–rubber transition or liquid crystalline transition. While many SMPs have been explored, poly(ϵ -caprolactone) (PCL)-based SMPs have been utilized as a biomaterial due to their well-characterized biocompatibility [9] and biodegradability [10,11]. Combining SMPs with various fabrication processes has resulted in diverse structures including shape-memory films, foams, particles,

surfaces, and fibers [4,12–19]. Particularly, SMPs in the form of fibers are generating great interest in structural and functional applications owing to their extremely high surface area, porous structure, and filtration/penetration properties [20–24]. Various thermoplastic polymers have been spun into nanofibers by the electrospinning method, which has been extensively acknowledged as an efficient and convenient approach for producing nanofibrous materials [24,25]. Fibrous materials are attractive as tissue engineering scaffolds because of their ability to enhance cell attachment, control pore architecture and create a 3-D microenvironment that encourages cell–cell contact [26,27]. Fibrous scaffolds have been implemented in cardiovascular [28–30], musculoskeletal [31,32], neural [33], and stem cell tissue engineering [34,35]. In addition, submicron-diameter fibers can provide tissue-matching mechanical compliance and provide topographic cues similar to that of native extracellular matrices (ECM). Studies have revealed that ECM topography greatly alters cell differentiation and tissue function [36–39].

Numerous studies have demonstrated the processable and structural advantages of nanofibrous materials with shape-memory properties. Matsumoto et al. using poly(ω -pentadecalactone) and PCL shape-memory microfibers achieved a strain recovery rate (R_r) of >89% and a strain fixity rate (R_f) of >82% by applying small deformations (~25%) [40]. Fejős et al. generated triple-shape memory nanofibers to study the effect of the structure on triple-shape memory by exploiting the T_g of epoxy and the T_m of PCL as the shape-switching temperatures [41]. Good strain recovery rates (>94% for T_g and >89% for T_m) were obtained; however the samples were deformed to only 2% strain. Ji et al. developed a series of shape-memory polyurethanes with varying soft-hard segment ratios [42]. The R_f increased from 75% to 92% and the R_r decreased from 92% to 85% with increasing hard segment contents. Barmouz et al. investigated the shape memory behavior of poly(lactic acid)-thermoplastic polyurethane/cellulose-nanofiber bio-nanocomposites. They concluded that through the addition of cellulose nanofibers, stress recovery of >40% could be achieved with little change in strain recovery [43]. Kawaguchi et al. found that by combining chitosan fibers with polyether-based thermoplastic polyurethane, the crystal structure gradually changed from semi-crystalline to amorphous state despite little or no change to the glass transition temperature. The elastic module of this hybrid material increased by 40% as compared with pure thermoplastic polyurethane. Shape recovery of these materials could be achieved at temperatures ranging from 25 to 70 °C. [44]. Aslan et al. reported that shape polyurethane fibers prepared by wet spinning demonstrated R_f and R_r of 71% and 91%, respectively [45]. Although these values are considered good for the shape-memory behavior, shape-memory nanofibers generally show relatively lower shape fixity and recovery properties as compared with shape-memory films. One of the major reasons is its polymer network architecture. In general, SMP systems can be broadly classified into two types based on the network architecture: (1) a physically cross-linked network and (2) a covalently cross-linked network [46]. Because it is difficult to cross-link the networks chemically during electrospinning, physical cross-linking is more suitable for electrospun nanofiber systems. However, compared with chemical cross-linking, physical cross-linking generally results in less structurally stable networks.

In this study, we describe the rational design of shape-memory nanofiber meshes generated by electrospinning PCL-based polyurethane which demonstrate higher shape-memory abilities. A series of polyurethanes with different ratios of soft and hard segments were prepared. Hard segments participate in hydrogen bonding and crystallization conferring rigidity, while, soft segments demonstrate a reversible phase transformation at the T_m , conferring shape-memory properties. Altering the ratio of hard and soft segments in a single mesh resulted in dramatic differences in fiber processability, mechanical properties, T_m , and fiber stability. Systematic variations of these parameters resulted in deformations greater than or equal to 400%. In addition, we examined the control of cell orientation on the nanofiber meshes with different fiber alignments because controlling cell alignment is one of the most crucial steps to creating practical tissue scaffolds such as cardiovascular, musculoskeletal, neural areas because many cells in these tissues align well along the ECM. Also, recent studies in mechanobiology field have revealed that ECM topography greatly alter cell differentiation

and tissue function [14]. The polymer design strategy applied in this study can increase the prospective applications of shape-memory fibers in the biomedical field.

2. Materials and Methods

2.1. Materials

HDI, BD, ϵ -caprolactone (CL), and 1,1,1,3,3,3-hexafluoro-2-propanol (HFIP) were obtained from Tokyo Chemical Industry Co., Ltd. (Tokyo, Japan). Tin (II) 2-ethylhexanoate, rhodamine phalloidin, 4',6-diamidino-2-phenylindole dihydrochloride (DAPI), fibronectin, and 0.1% triton X-100 were purchased from Sigma-Aldrich Japan (Tokyo, Japan). Phosphate buffered saline (PBS) was purchased from Nakalai Tesque (Kyoto, Japan). Xylene, *n*-hexane, diethylether, tetrahydrofuran (THF), and paraformaldehyde were obtained from FUJIFILM Wako Pure Chemical Corporation (Osaka, Japan). Human mesenchymal stem cells (hMSCs) were purchased from Lonza (Basel, Switzerland).

2.2. Polymerization and Characterization

BD (194 μ L, 2.2 mmol) as an initiator was dried in vacuum overnight in a 300 mL round-bottom flask. CL (46.3 mL, 0.44 mol) was added into the flask and stirred under a N_2 atmosphere. Five drops of tin (II) 2-ethylhexanoate as a catalyst (5 droplets, 0.5 mmol) was then dropwise added and stirred at 120 $^{\circ}$ C for 24 h. The product was then completely dissolved in THF. The obtained PCL was purified by reprecipitation from hexane and diethyl ether. Then, 800 mg of purified PCL and 20 mL of xylene were added into a 50 mL sample tube and stirred at 60 $^{\circ}$ C for 15 min. HDI and tin (II) 2-ethylhexanoate were then added into the mixture and stirred at 60 $^{\circ}$ C for 30 min followed by the addition of BD. The added amounts of HDI and BD were 44 μ L (0.27 mmol) and 16 μ L (0.18 mmol), 58 μ L (0.36 mmol) and 24 μ L (0.27 mmol), and 72.5 μ L (0.45 mmol) and 32 μ L (0.36 mmol) to obtain PCL:HDI:BD molar ratios of 1:3:2, 1:4:3, and 1:5:4 (soft:hard segment = 1:5, 1:7, and 1:9), respectively. After stirring at 60 $^{\circ}$ C for 3 h, the mixture was purified by reprecipitation with a mixed solution of hexane and chloroform (80:3). The obtained polymer was filtered and dried in vacuum. The structures were determined by 1 H-nuclear magnetic resonance (NMR) spectroscopy (JEOL, Tokyo, Japan) with $CDCl_3$ as a solvent (Figure S1). Urethane bonds were analyzed by Fourier transform-infrared spectroscopy (FT-IR) (JEOL, Tokyo, Japan) with KBr pellet (Figure S2). The molecular weights were determined by Gel permeation chromatography (GPC) equipped with TSKgel G4000Hhr and TSKgel G3000Hhr columns and a refractive detector using *N,N*-dimethylformamide (DMF) with 10 mM LiCl as the eluent and solvent (0.8 mL/min, 40 $^{\circ}$ C) (HLC-8220GPC, Tosho Corporation, Tokyo, Japan) (Table 1).

Table 1. Characteristic data of a series of PCL-based polyurethanes. PDI: Polydispersity index.

Samples	Composition (Molar Ratio)	Segment Ratio ¹⁾ (Molar Ratio)		Segment Ratio (w/w%)		Feed			Molecular Weight ²⁾		PDI ²⁾
		Soft	Hard	Soft	Hard	PCL (mg)	HDI (μ L)	BD (μ L)	M_w	M_n	
PCL	-	-	-	-	-	-	-	-	59,700	46,300	1.29
PCL-6.8	1:3:2	1	5	93.2	6.8	800	44	16	78,900	54,000	1.46
PCL-9.2	1:4:3	1	7	90.8	9.2	800	58	24	73,200	53,000	1.38
PCL-11.3	1:5:4	1	9	88.7	11.3	800	73	32	93,500	68,000	1.37

¹⁾ Soft:Hard = PCL:HDI + BD (PCL; poly(ϵ -caprolactone), HDI; hexamethylene diisocyanate, BD;1,4-butanediol).

²⁾ Measured by GPC.

2.3. Electrospinning Method and Characterization of Nanofibers

The electrospinning solution was prepared by dissolving the polymer in HFIP (40 w/v%). PCL with different ratios of HDI and BD were electrospun into nanofibers using an applied voltage of 25 kV, a needle gauge of 23, a flow rate of 0.5 mL/h, and a 15 cm separation between the needle and the collector plate (Nanon-01A, MECC Co., Ltd., Fukuoka, Japan) (n = 3). The formation of

electrospun nanofibers was observed using a scanning electron microscope (SEM; SU8000, Hitachi High-Technologies Corporation, Tokyo, Japan). The thermal property of the nanofibers with different ratios of HDI and BD was measured by differential scanning calorimetry (DSC; 6100, SEIKO Instruments, Chiba, Japan) at a heating/cooling rate of 5 °C/min. For the thermal stability test, a nanofiber mesh with a soft:hard segment ratio of 1:5, 1:7, or 1:9 was placed in an oven at 60 °C for 24 h. The nanofiber morphology before and after heating was compared by SEM observation. Because polyurethanes are known as hygroscopic material, we have conducted all experiments under constant temperature/humidity conditions (21 °C/25%).

2.4. Shape Memory Behavior

The shape memory effect of the electrospun nanofibers with a soft:hard segment ratio of 1:7 was evaluated in terms of morphology, diameter change, orientation, and shape recovery rate of the nanofibers before deformation, after deformation, and after shape memory recovery. The nanofiber was first heated at 60 °C in water and then stretched to a temporary shape. The nanofiber was reheated at 60 °C, which led to shape recovery. The formation of nanofibers and their morphologies before deformation, during formation of the temporary shape, and after shape recovery were observed by SEM. The surface and cross-section of the shape memory fiber were observed. From the magnified cross-sectional and top-view images, the diameters of the nanofiber before deformation, during formation of the temporary shape, and after shape recovery were calculated. The orientation of the nanofibers before and after deformation, and after shape recovery was analyzed, and the orientation images were created by Image J software (Image J, the National Institutes of Health, Bethesda, MD, USA) using the plugin orientation J to obtain direction distribution maps and their histograms (Figure S3). The R_r and R_f were calculated by cutting the shape memory nanofiber to 1 cm length and comparing the length of the nanofiber before deformation and shape recovery ($n = 3$). The strain fixity rate describes the ability to fix the mechanical deformation as $R_f(N) = \varepsilon_f(N) / \varepsilon_m \times 100\%$. The strain recovery rate was the ability of the material to recover its permanent shape, which calculated from $R_r = (\varepsilon_m - \varepsilon_r(N)) / \varepsilon_m - \varepsilon_r(N - 1) \times 100\%$ (ε_m ; max strain, ε_r ; recovered strain, ε_f ; final strain after deformation, N is the number of cycles). The nanofiber was heated at 60 °C in water, and then stretched to a certain elongation degree (200%, 300%, or 400%). The nanofiber was again placed in water at 60 °C for shape memory recovery. The recovery stress of PCL-9.2 nanofiber was also measured through a tensile test (EZ-S, SHIMADZU, Kyoto, Japan). At first, the sample was extended to 150% elongation over 60 °C in chamber (M-600FN, TAITEC, Saitama, Japan) and then, the sample was cooled down to 0 °C. The sample was maintained at the constant deformation for 1 hour. Subsequently, the sample was reheated to 60 °C and the stress stored in the sample was released. The largest value was taken as the representative of the recovery stress at this strain (Figure S4).

2.5. Cell Culture on Nanofiber Mesh

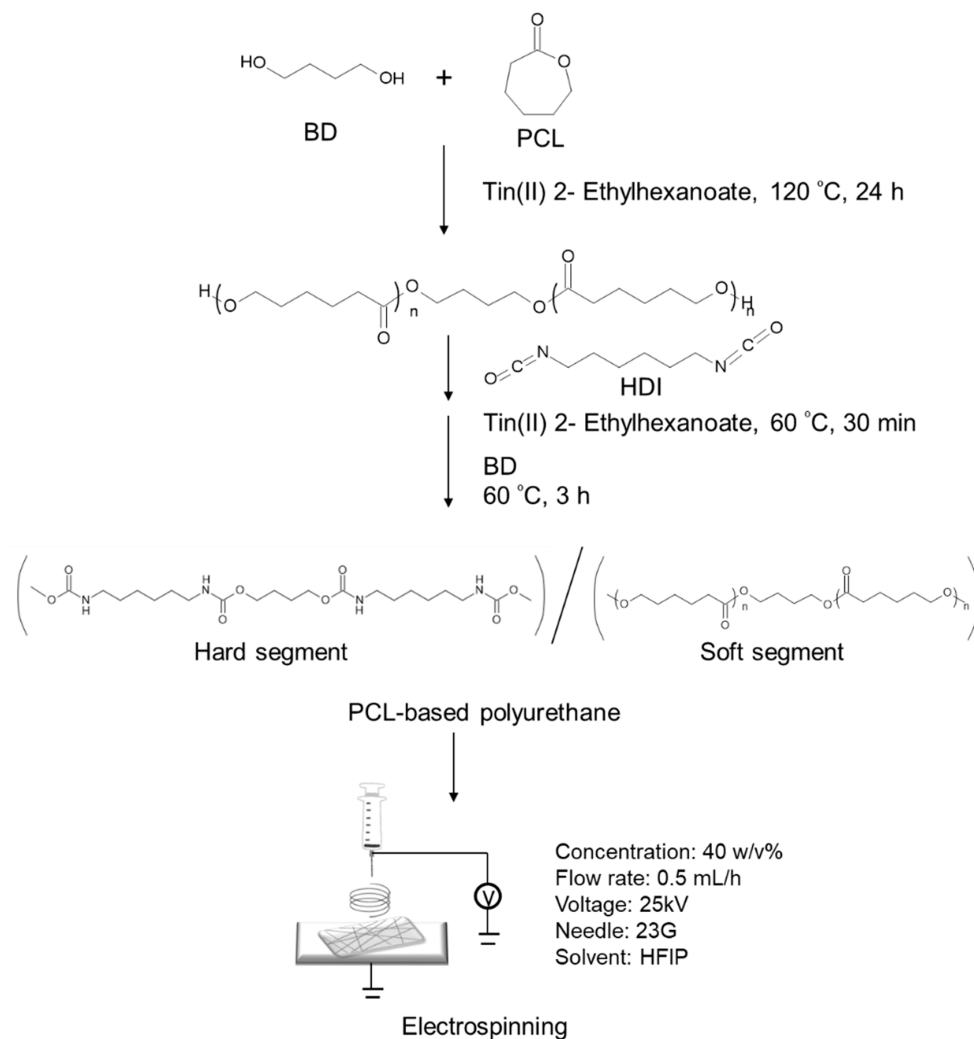
Before starting the hMSC culture, the original and temporarily stretched electrospun nanofibers with a soft:hard segment ratio of 1:7 were sterilized by ultraviolet (UV) irradiation for 15 min. The nanofibers were coated with 20 $\mu\text{g mL}^{-1}$ fibronectin for 1 h at 37 °C. After washing with PBS, hMSCs were seeded at a density of 5000 cells cm^{-2} on the sterilized nanofiber and cultured in a hMSC growth medium (MSCGMTM, Lonza, Basel, Switzerland) for 1 day. The hMSCs cultured on the nanofibers were fixed using 4% paraformaldehyde for 15 min and then permeabilized using 0.1% Triton X-100 for 5 min. Cells were stained using rhodamine phalloidin and DAPI to visualize F-actin and nuclei respectively. Finally, the cell morphology on the nanofiber meshes was imaged using a fluorescence microscope (ECLIPSE Ti2, Nikon, Tokyo, Japan). The phase contrast and fluorescence images were taken for cells and nanofibers in the same field. Finally, three images including phase contrast (nanofibers and cells), fluorescence images for nucleus (DAPI) and F-actins (Phalloidin) from the same field were merged. To investigate the overview of cellular alignment, large field scan was also performed. All original images were shown in Figure S5. Cell viability on the nanofiber meshes

before and after deformation was evaluated using Alamar blue. The metabolic activity of hMSCs cultured on nanofiber meshes before and after deformation as well as on glass substrates was assessed ($n = 4$). Briefly, cells were treated with Alamar blue reagent diluted in culture media (10%) for 4 hours at 37 °C. Media was then sampled and analyzed using a fluorescence plate reader (PerkinElmer Co., Ltd., Kanagawa, Japan).

3. Results

3.1. Fabrication of Poly(ϵ -Caprolactone) PCL-Based Polyurethane Nanofiber Meshes

Three different PCL-based polyurethanes were synthesized by reacting a PCL diol (generated by a caprolactone ring opening polymerization [2,13,15]), 1,4-butanediol (BD) and hexamethylene diisocyanate (HDI) (Scheme 1) in varying soft:hard segment ratios (1:5, 1:7, and 1:9 corresponding to PCL:HDI:BD molar ratios of 1:3:2, 1:4:3, and 1:5:4, respectively). Polymer synthesis was then confirmed by $^1\text{H-NMR}$ spectroscopy and gel permeation chromatography (GPC) (Figure S1 and Table 1). Soft:hard segment ratios of 1:5, 1:7, and 1:9 resulted in polymers containing roughly 6.8, 9.2, and 11.3 w/w% of hard segments and were thus abbreviated PCL-6.8, PCL-9.2 and PCL-11.3. Urethane peaks were detected from $^1\text{H-NMR}$ spectrum at 3.2 ppm and FT-IR spectrum as C–N stretching and N–H bending at 1540 cm^{-1} , bending vibrations of the N–H bond at 1580 cm^{-1} , and free amide group (–NH–) peak at 3340 cm^{-1} (Figure S1 and S2) [47].



Scheme 1. Synthesis of poly(ϵ -caprolactone) (PCL)-based polyurethanes and fabrication of nanofiber mesh by electrospinning.

As molecular weight is a critical factor for electrospinning and intermolecular chain entanglement is necessary, number-average molecular weight (M_n) was closely monitored. Figure S6 shows the morphology of the electrospun PCL with a molecular weight of 5000. Here we observe that at low molecular weights beads or particles can form due to insufficient molecular chain entanglement during the fiber fabrication process. We and others have found that polymers with $M_n < 10,000$ form bead-like structures, while polymers with a relatively higher M_n ($>50,000$) form fibers during electrospinning at a low solution concentration [48]. All three PCL-based polyurethanes generated in this work demonstrated a number-average molecular weights of 50,000 and more, well within the expected electrospinning fiber forming range.

Solution concentration, applied electric field, and distance between the spinneret and collectors are also important factors which can be tuned to change nanofiber structure and were therefore optimized. All samples showed good processability at a concentration of 40 w/v%. As shown in Figure 1, smooth fibrous structures without beads were formed with average diameters of 417 ± 20 , 511 ± 30 , and 1329 ± 61 nm for PCL-6.8, PCL-9.2, and PCL-11.3, respectively. Interestingly, polymers with extremely low ($<4.4\%$) or high ($>21.3\%$) hard segment contents did not form consistent fiber structures. Electrospinning PCL-21.3 resulted in a bead-like structure rather than a fiber mesh (Figure S7). This is because polymer chains tend to aggregate as the hard segment amount increases. In addition to polymer composition, polymer architecture is also considered an important factor in electrospinning. Figure S8 shows the SEM images of the electrospun fibers from the four-branched PCL. Even though the molecular weight is similar, no fiber structures were formed.

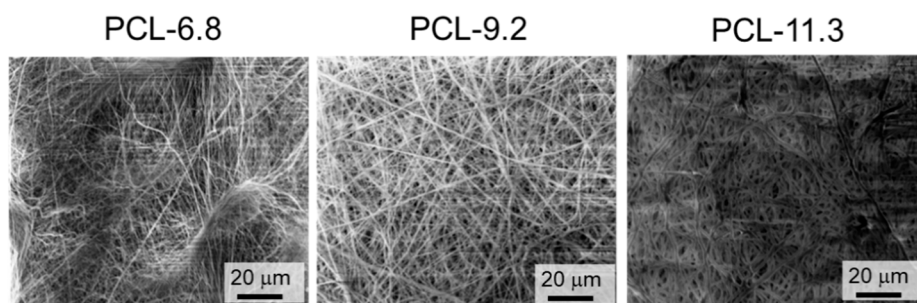


Figure 1. Scanning electron microscope (SEM) micrographs of fibers electrospun from PCL-6.8, 9.2, and 11.3 (10 kV accelerating voltage).

3.2. Thermal Properties

The thermal properties of the nanofibers were characterized by differential scanning calorimetry (DSC) (Figure 2). The peak attributed to hard segment was observed around $150\text{ }^{\circ}\text{C}$ (Figure S9) [49]. Interestingly, the T_m of all three nanofiber meshes were slightly lower than that of the corresponding pure PCL nanofiber mesh suggesting disruption of polymer crystallization through hydrogen bonding between the hard segments [50]. In the case of nanofibers, this trend becomes more significant because the molecular orientation generated during the spinning process can lead to the alignment of polyurethane molecules along the fiber axis. The preferred orientation of the molecules leads to the packing and aggregation of hard segments into hard-segment microdomains. As a result, the differences in T_m between linear PCL and the PCL-based polyurethanes are accentuated. We also evaluated the crystallization of PCL-based polyurethanes by cooling scan of DSC (Figure S10). The exothermic peaks of PCL, PCL-6.8, PCL-9.2, and PCL-11.3 were found around $30\text{ }^{\circ}\text{C}$, $30\text{ }^{\circ}\text{C}$, $38\text{ }^{\circ}\text{C}$, and $36\text{ }^{\circ}\text{C}$, respectively. Although the crystallization temperature of polyurethanes was higher than that of pure PCL, heat of crystallization decreased as hard segment was introduced.

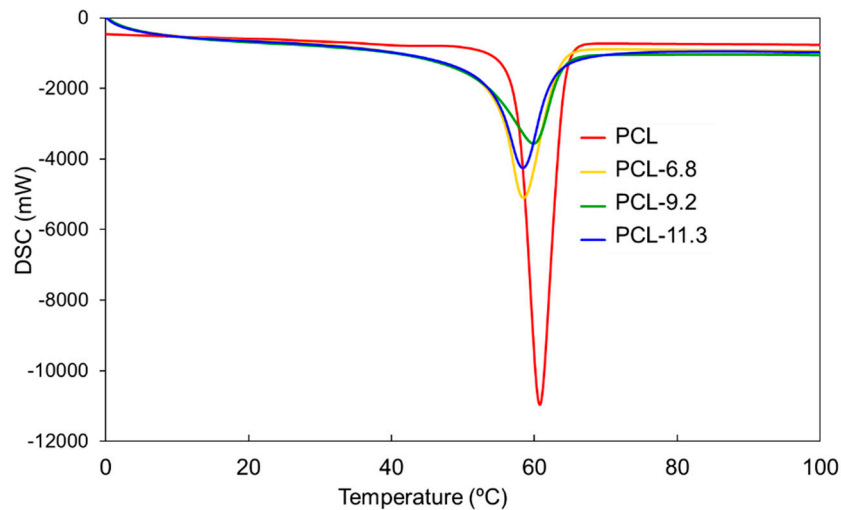


Figure 2. Differential scanning calorimetry (DSC) curves of electrospun fibers of pure PCL and PCL-6.8, 9.2, and 11.3.

To confirm the thermostability of the physically cross-linked polyurethane samples, samples were heated to near their T_m (around 60 °C) and their morphologies were analyzed by SEM. Figure 3 presents the SEM images before and after heating (magnified images was shown at Figure S11). Before heating, all the nanofibers showed the formation of uniform fibers. After heating, PCL-6.8 was melted, whereas PCL-9.2 and PCL-11.3 retained their fibrous morphologies. This result indicates that the physical cross-linking within PCL-6.8 was insufficient to maintain its morphology above its T_m . On the other hand, PCL-21.3 (>21.3%) broke after heating even though it had the highest hard segment content (Figure S12). These results suggest that careful selection of a soft:hard segment ratio is important for designing high-performance shape-memory nanofibers.

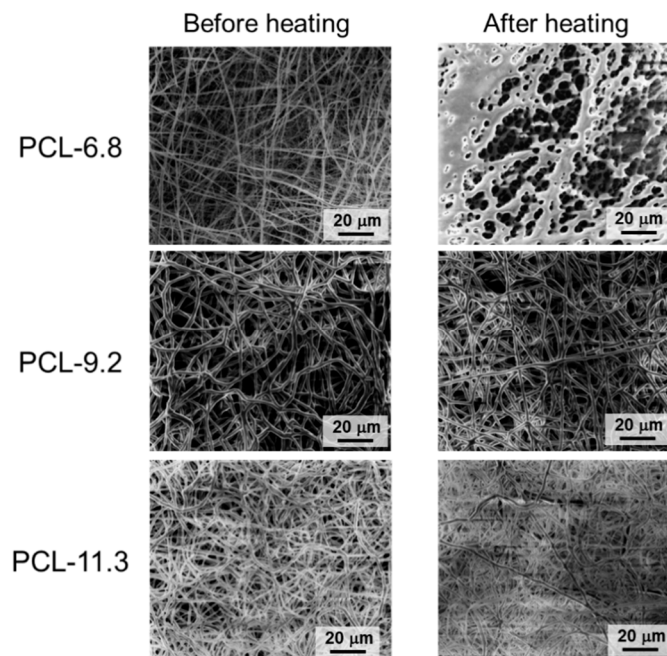


Figure 3. SEM micrographs of electrospun fibers of PCL-6.8, 9.2, and 11.3 before and after heating at 60 °C for 24 h.

3.3. Shape-Memory Properties

The shape memory capabilities of the nanofiber mesh were assessed by SEM and orientation analyses. Figure 4a shows digital camera, SEM, and cross-sectional images of PCL-9.2 nanofibers before deformation, after 300% deformation and fixation, and after shape recovery. The fibers showed different structures before and after deformation. The original, randomly oriented fibrous structure was easily deformed into a temporary stretched shape wherein fibers tended to orient along the strain direction. The oriented fibers recovered their original structure when the sample was reheated. Cross-sectional images of PCL-9.2 nanofibers during the shape memory cycle demonstrate that mean fiber diameter slightly decreased from around 600 nm to 500 nm after stretching (Figure 4b), and that the cross-sectional shape changed slightly from circular to ellipsoidal after stretching. Following shape recovery, the mean fiber diameter recovered to around 700 nm. The nanofiber structure was also stable after the shape memory test cycles at a microscopic level. Figure 4c presents a comparison between the R_f and R_r of the PCL-9.2 nanofiber mesh under different deformation rates (200, 300, and 400%). The R_f values were 88, 90, and 93%, and the R_r values were 100, 89, and 91% after 200, 300, and 400% deformation, respectively. In this study, we only showed PCL-9.2 data because PCL-6.8 melted above 60 °C, while PCL-11.3 is fragile and easily broken.

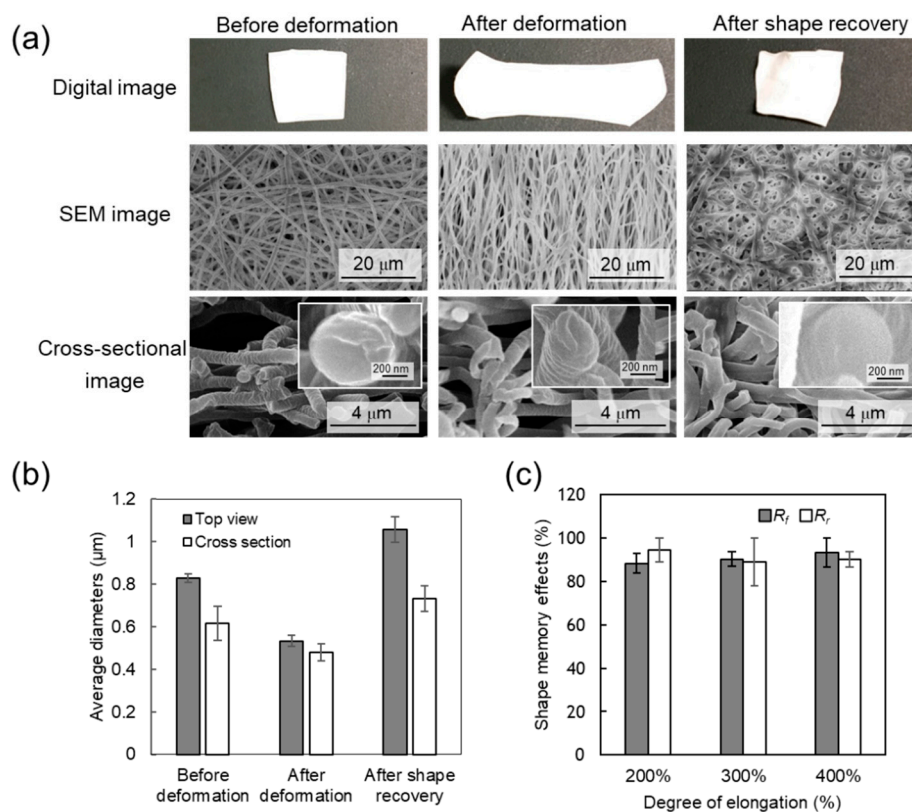


Figure 4. Evaluations of shape-memory effect of PCL-9.2 nanofibers. (a) Digital (top) and SEM (middle and bottom) images of PCL-9.2 nanofibers before deformation (left), after deformation (middle), and after shape memory recovery (right). (b) Average diameters of PCL-9.2 nanofibers calculated from the cross-sectional images before deformation, after deformation, and after shape memory recovery (n = 3). (c) Shape fixity rate (R_f) and recovery rate (R_r) of PCL-9.2 nanofibers under different elongation degrees (200%, 300%, and 400%) (n = 3).

To visualize the fiber orientation during the shape memory cycle, orientation analysis was performed using image analysis software (n = 3). The software evaluated the structure tensor of each Gaussian-shaped window by computing the continuous spatial derivatives in the x and y dimensions using Gaussian interpolation. For qualitative visual representation of the orientation, the grey-scale

SEM images were converted into color-coded images (Figure 5a). The fibers oriented along the deformation direction were assigned a $\pm 90^\circ$ orientation. The fiber orientation was clearly observed. For quantitative assessment, the average population of different orientation distributions of the fibers is presented in Figure 5b.

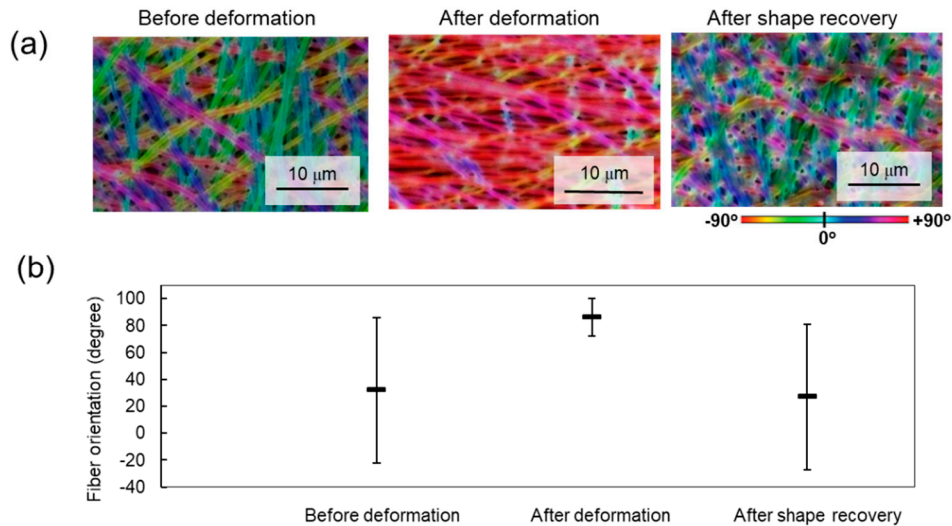


Figure 5. Orientation analysis of PCL-9.2 nanofibers before deformation, after deformation, and after shape memory recovery. (a) SEM images analyzed by Image J software for orientation evaluation and (b) fiber orientation distribution of nanofibers before deformation, after deformation, and after shape recovery.

3.4. Cellular Alignment

Matrix and scaffold topography are known to alter cell morphology and orientation. Recent studies have demonstrated that mesenchymal stem cells (MSCs) can sense the mechanical properties of their underlying culture substrate through integrin and focal adhesion kinase signaling to reorganize their actin cytoskeleton in response to extrinsic mechanical signals [18,48]. Therefore, we assessed the potential of our shape-memory nanofiber meshes to influence the MSC morphology. Human mesenchymal stem cells (hMSCs) were seeded onto the PCL-9.2 nanofiber mesh with and without deformation (300%). The cells on the random fiber mesh (non-stretched) spread extensively but with a random orientation (Figure 6), whereas the cells on the aligned fiber mesh (stretched) elongated along the fiber axis. The cells were seeded on the nanofiber before deformation and after shape recovery, respectively. Cellular alignments were then compared between these two conditions. Due to the long fibrous structure of the nanofibers, cells upon adhesion are geometrically restricted in the direction and orientation in which they can spread. Consequently, internal cellular structures like the cell cytoskeleton reflect the underlying material anisotropy resulting in cell alignment along the dominant fiber direction [51]. The cells cultured on the nanofibers were still alive after 2 days and the cell viabilities were similar to that on control substrate (glass substrate) (Figure S13). In this study, we cultured cells on the nanofiber before deformation or after deformation. Therefore, the effect of temperature was not considered. However, to observe how cells respond to dynamic change of the substrate during shape-memory activation is more attractive from the viewpoint of a mechanobiology study. Therefore, the next step of this study is to adjust the shape-switching temperature of fibers to 37 °C and examine dynamic cell culture on them. The shape-switching temperature of SMP can be possibly controlled by its molecular nanoarchitecture such as molecular weight, branched structure, hard/soft segment ratio etc [52].

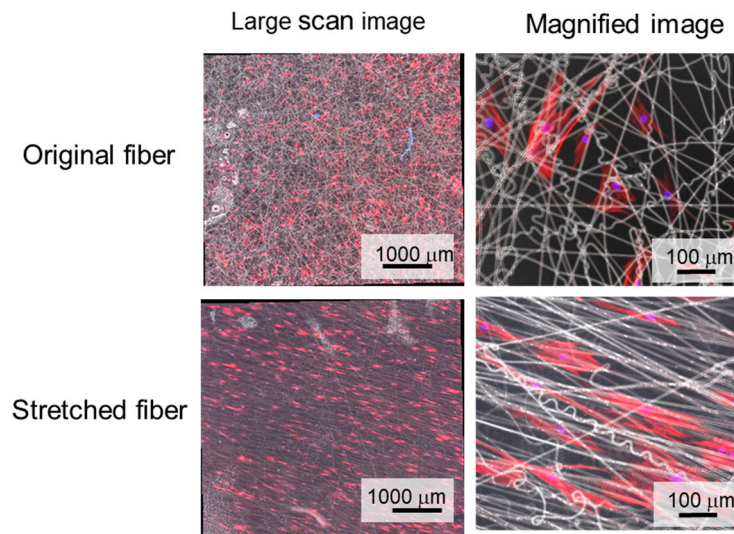


Figure 6. Adhesion morphology and alignment of human mesenchymal stem cells (hMSCs) on original (left) and stretched (right) PCL-9.2 nanofibers. hMSCs on each fiber type were stained with f-actin (red) and nucleus (blue). hMSCs were cultured at 37 °C for 24 h. Large scan (left) and magnified (right) images show global and local alignment of hMSCs.

4. Discussion

Thermally induced shape memory effect has the ability to recover their permanent shape from a temporary shape in response to biologically relevant temperature changes [13–15,17], thereby enabling the development of shape-memory cell culture substrates [13–15,17]. Nanopatterns can be programmed by mechanically embossing the desired topography into the polymer surface. Previous studies have demonstrated that cells cultured on these shape-memory surfaces can reorganize their cytoskeletons as well as alter their contractile direction in response to changes in material topography [39]. These studies have drawn much attention as they demonstrate a novel class of dynamic cell culture platforms to better understand the relationship between mechanical stresses and biological functions in a time-dependent manner. Through this work, it has been recognized that the mechanical interactions between cells and their extracellular matrix can regulate cell fate. In other words, cellular mechanisms are described whereby cells could sense, measure and respond to the space they were in, in particular to the rigidity of the surface the cells were on. By altering topographical cues in a controlled manner, these platforms enable researchers to recapitulate the dynamic nature of physiological conditions like wound healing, organogenesis and tumorigenesis in a dish. We also developed shape-memory microparticles by an in situ oil-in-water emulsion polymerization technique [16]. The particles with a disk-like temporal shape recovered their original spherical shape upon heating. Such particles can be potentially used for bioseparation, and in future, for drug delivery and immune engineering. In this study, shape-memory nanofiber meshes were prepared by electrospinning. Interestingly, polymers with extremely low or high soft:hard segment ratios were unable to form reproducible fibers as they demonstrated too few or too many inter-/intra-polymer interactions or entanglements. Smooth fibrous structures were successfully formed from PCL-6.8, 9.2, and 11.3, although PCL-6.8 melted after being heated above the T_m because the physical cross-linking within PCL-6.8 was insufficient to maintain its morphology.

To discuss the detailed mechanism of the shape-memory nanofibers, the microscopic shape-memory properties were considered. As hypothesized, the hard segments governed the mechanical properties of the permanent shape of the polymer network, and the soft segments as the reversible phase permitted shape memory properties. If the sample temperature exceeds the T_m , the crystalline region of the molecular chains will melt allowing one to be deformed. If the nanofiber meshes are stretched, the molecular chains will extend. Upon cooling to below the T_m , the molecular

chains will crystallize. Resultantly, internal stress is stored in the extended fibers as the mesh is maintained in an intermediate semi-crystalline state. After reheating to above the T_m , the molecular chains become flexible and the nanofiber mesh recovers its original shape. Therefore, as hard segment content increased, shape fixity increased and shape recovery ratios decreased gradually. In this work, the fibers subjected to the deformation and recovery processes demonstrated microscopic changes in fiber structure as observed by SEM which matched macroscopic changes visible by eye. These results indicated that the shape-memory properties of the nanofibers were substantially determined by the internal structure of the PCL-based polyurethane but not by the macroscopic structural changes within the non-woven fabric. Compared to other shape-memory forms, many factors need to be considered to design shape-memory nanofibers. For example, fibrous materials have higher porosity, which can provide a low shape fixity ratio. It has also been proven that the electrospinning process produces a partial molecular orientation that can lead to an increase in the amount of the hard-segment phase, resulting in an increased recovery stress. However, the increase in the recovery stress adversely affected the fixing of the temporary shape, and thus, the shape fixity decreased. We also evaluated the recovery stress of PCL-9.2 after shape-memory activation. The value obtained from a tensile test was around 11 MPa (Figure S4). This value is relevant to previously reported values [42].

These unique and tunable aspects of shape-memory nanofibers may make them uniquely suitable for many biomedical applications. For example, their rapid recovery might be utilized in stents and endovascular thrombectomy devices in surgical approaches. In contrast, a slower recovery rate would provide an opportunity to study the long-term effect of dynamic matrix structure changes on cell behaviors such as cell differentiation and proliferation. Although here we only demonstrate cell culture on the shape-memory meshes before and after deformation, we believe that shape-memory meshes with transition temperatures within cytocompatible ranges may be utilized to control cell behavior through dynamic shape-memory changes.

5. Conclusions

We reported a novel strategy for the facile production of shape-memory nanofiber meshes. As demonstrated, smooth fibrous structures without beads were formed from PCL-based polyurethanes with different soft-to-hard segment ratios. The original nanofibrous structure easily deformed into a temporary shape, and recovered its original structure when the sample was reheated. A significantly high recovery rate (>89%) was obtained even when the mesh was deformed up to 400%. Furthermore, hMSCs aligned well along the fiber orientation when they were cultured on the meshes. Owing to their good biocompatibility, the proposed shape-memory nanofiber system would provide an opportunity to study the effect of dynamic matrix structure changes on cell behaviors. Moreover, another advantage of electrospinning is the possibility of encapsulating drugs in the fibers.

Supplementary Materials: The following are available online at <http://www.mdpi.com/2079-6439/7/3/20/s1>.

Author Contributions: Conceptualization, M.E.; Methodology, K.U.; Software, K.U., E.N., and K.T.; Formal Analysis, K.T.; Investigation, K.T.; Resources, M.E.; Data Curation, K.T. and E.N.; Writing-Original Draft Preparation, E.N.; Writing-Review and Editing, K.U., M.E., and A.K.; Supervision, M.E.; Project Administration, M.E.; Funding Acquisition, M.E.

Funding: This research was funded by JSPS KAKENHI (Grant Number 264086 and 26750152).

Acknowledgments: The authors thank the support from Namiki Foundry at National Institute for Materials Science (NIMS) for SEM measurements.

Conflicts of Interest: The authors declare no conflict of interest.

References

1. Gall, K.; Dunn, M.L.; Liu, Y.; Finch, D.; Lake, M.; Munshi, N.A. Shape memory polymer nanocomposites. *Acta Biomater.* **2002**, *50*, 5115–5126. [[CrossRef](#)]
2. Lendlein, A.; Langer, R. Biodegradable, elastic shape-memory polymers for potential biomedical applications. *Science* **2002**, *296*, 1673–1676. [[CrossRef](#)] [[PubMed](#)]
3. Nagahama, K.; Ueda, Y.; Ouchi, T.; Ohya, Y. Biodegradable shape-memory polymers exhibiting sharp thermal transitions and controlled drug release. *Biomacromolecules* **2009**, *10*, 1789–1794. [[CrossRef](#)] [[PubMed](#)]
4. Hu, J.; Zhu, Y.; Huang, H.; Lu, J. Recent advances in shape-memory polymers: Structure, mechanism, functionality, modeling and applications. *Prog. Mater. Sci.* **2012**, *37*, 1720–1763. [[CrossRef](#)]
5. Liu, Y.; Du, H.; Liu, L.; Leng, J. Shape memory polymers and their composites in aerospace applications: A review. *Smart Mater. Struct.* **2014**, *23*, 023001. [[CrossRef](#)]
6. Wang, J.; Quach, A.; Brasch, M.E.; Turner, C.E.; Henderson, J.H. On-command on/off switching of progenitor cell and cancer cell polarized motility and aligned morphology via a cytocompatible shape memory polymer scaffold. *Biomaterials* **2017**, *140*, 150–161. [[CrossRef](#)] [[PubMed](#)]
7. Tseng, L.F.; Mather, P.T.; Henderson, J.H. Shape-memory-actuated change in scaffold fiber alignment directs stem cell morphology. *Acta Biomater.* **2013**, *9*, 8790–8801. [[CrossRef](#)] [[PubMed](#)]
8. Bothe, M.; Emmerling, F.; Pretsch, T. Poly(ester urethane) with Varying Polyester Chain Length: Polymorphism and Shape-Memory Behavior. *Macromol. Chem. Phys.* **2013**, *214*, 2683–2693. [[CrossRef](#)]
9. Hsu, S.-H.; Hung, K.-C.; Lin, Y.-Y.; Su, C.-H.; Yeh, H.-Y.; Jeng, U.S.; Lu, C.-Y.; Dai, S.A.; Fu, W.-E.; Lin, J.-C. Water-based synthesis and processing of novel biodegradable elastomers for medical applications. *J. Mater. Chem. B* **2014**, *2*, 5083–5092. [[CrossRef](#)]
10. Chien, Y.C.; Chuang, W.T.; Jeng, U.S.; Hsu, S.H. Preparation, Characterization, and Mechanism for Biodegradable and Biocompatible Polyurethane Shape Memory Elastomers. *ACS Appl. Mater. Interfaces* **2017**, *9*, 5419–5429. [[CrossRef](#)] [[PubMed](#)]
11. Takahashi, T.; Hayashi, N.; Hayashi, S. Structure and Properties of Shape-Memory Polyurethane Block Copolymers. *J. Appl. Polym. Sci.* **1996**, *60*, 1061–1069. [[CrossRef](#)]
12. Leng, J.; Lan, X.; Liu, Y.; Du, S. Shape-memory polymers and their composites: Stimulus methods and applications. *Prog. Mater. Sci.* **2011**, *56*, 1077–1135. [[CrossRef](#)]
13. Ebara, M.; Uto, K.; Idota, N.; Hoffman, J.M.; Aoyagi, T. Shape-memory surface with dynamically tunable nano-geometry activated by body heat. *Adv. Mater.* **2012**, *24*, 273–278. [[CrossRef](#)] [[PubMed](#)]
14. Ebara, M.; Akimoto, M.; Uto, K.; Shiba, K.; Yoshikawa, G.; Aoyagi, T. Focus on the interlude between topographic transition and cell response on shape-memory surfaces. *Polymer* **2014**, *55*, 5961–5968. [[CrossRef](#)]
15. Ebara, M.; Uto, K.; Idota, N.; Hoffman, J.M.; Aoyagi, T. The taming of the cell: Shape-memory nanopatterns direct cell orientation. *Int. J. Nanomed.* **2014**, *9*, 117–126. [[CrossRef](#)] [[PubMed](#)]
16. Uto, K.; Ebara, M. Magnetic-Responsive Microparticles that Switch Shape at 37 °C. *Appl. Sci.* **2017**, *7*, 1203. [[CrossRef](#)]
17. Uto, K.; Mano, S.S.; Aoyagi, T.; Ebara, M. Substrate Fluidity Regulates Cell Adhesion and Morphology on Poly(ϵ -caprolactone)-Based Materials. *ACS Biomater. Sci. Eng.* **2016**, *2*, 446–453. [[CrossRef](#)]
18. Uto, K.; Aoyagi, T.; DeForest, C.A.; Hoffman, A.S.; Ebara, M. A Combinational Effect of “Bulk” and “Surface” Shape-Memory Transitions on the Regulation of Cell Alignment. *Adv. Healthc. Mater.* **2017**, *6*, 1601439. [[CrossRef](#)] [[PubMed](#)]
19. Naheed, S.; Zuber, M.; Barikani, M. Synthesis and thermo-mechanical investigation of macrodiol-based shape memory polyurethane elastomers. *Int. J. Mater. Res.* **2017**, *108*, 515–522. [[CrossRef](#)]
20. Cha, D.; Kim, H.Y.; Lee, K.H.; Jung, Y.C.; Cho, J.W.; Chun, B.C. Electrospun nonwovens of shape-memory polyurethane block copolymers. *J. Appl. Polym. Sci.* **2005**, *96*, 460–465. [[CrossRef](#)]
21. Kotek, R. Recent advances in polymer fibers. *Polym. Rev.* **2008**, *48*, 221–229. [[CrossRef](#)]
22. Zhuo, H.; Hu, J.; Chen, S. Electrospun polyurethane nanofibres having shape memory effect. *Mater. Lett.* **2008**, *62*, 2074–2076. [[CrossRef](#)]
23. Chung, S.E.; Park, C.H.; Yu, W.-R.; Kang, T.J. Thermoresponsive shape memory characteristics of polyurethane electrospun web. *J. Appl. Polym. Sci.* **2011**, *120*, 492–500. [[CrossRef](#)]
24. Okada, T.; Niiyama, E.; Uto, K.; Aoyagi, T.; Ebara, M. Inactivated Sendai virus (HVJ-E) immobilized electrospun nanofiber for cancer therapy. *Materials* **2016**, *9*, 12. [[CrossRef](#)] [[PubMed](#)]

25. Garrett, R.; Niiyama, E.; Kotsuchibashi, Y.; Uto, K.; Ebara, M. Biodegradable nanofiber for delivery of immunomodulating agent in the treatment of basal cell carcinoma. *Fibers* **2015**, *3*, 478–490. [[CrossRef](#)]
26. Brannmark, C.; Paul, A.; Ribeiro, D.; Magnusson, B.; Brolen, G.; Enejder, A.; Forslow, A. Increased adipogenesis of human adipose-derived stem cells on polycaprolactone fiber matrices. *PLoS ONE* **2014**, *9*, e113620. [[CrossRef](#)] [[PubMed](#)]
27. Hyysalo, A.; Ristola, M.; Joki, T.; Honkanen, M.; Vippola, M.; Narkilahti, S. Aligned Poly(epsilon-caprolactone) Nanofibers Guide the Orientation and Migration of Human Pluripotent Stem Cell-Derived Neurons, Astrocytes, and Oligodendrocyte Precursor Cells In Vitro. *Macromol. Biosci.* **2017**, *17*, 1600517. [[CrossRef](#)] [[PubMed](#)]
28. Stitzel, J.; Liu, J.; Lee, S.J.; Komura, M.; Berry, J.; Soker, S.; Lim, G.; Van Dyke, M.; Czerw, R.; Yoo, J.J.; et al. Controlled fabrication of a biological vascular substitute. *Biomaterials* **2006**, *27*, 1088–1094. [[CrossRef](#)] [[PubMed](#)]
29. Stankus, J.J.; Guan, J.; Fujimoto, K.; Wagner, W.R. Microintegrating smooth muscle cells into a biodegradable, elastomeric fiber matrix. *Biomaterials* **2006**, *27*, 735–744. [[CrossRef](#)] [[PubMed](#)]
30. Xu, C.; Inai, R.; Kotaki, M.; Ramakrishna, S. Electrospun nanofiber fabrication as synthetic extracellular matrix and its potential for vascular tissue engineering. *Tissue Eng.* **2004**, *10*, 1160–1168. [[CrossRef](#)] [[PubMed](#)]
31. Riboldi, S.A.; Sampaolesi, M.; Neuenschwander, P.; Cossu, G.; Mantero, S. Electrospun degradable polyesterurethane membranes: Potential scaffolds for skeletal muscle tissue engineering. *Biomaterials* **2005**, *26*, 4606–4615. [[CrossRef](#)] [[PubMed](#)]
32. Shields, K.J.; Beckman, M.J.; Bowlin, G.L.; Wayne, J.S. Mechanical properties and cellular proliferation of electrospun collagen type. *Tissue Eng.* **2004**, *10*, 1510–1517. [[CrossRef](#)] [[PubMed](#)]
33. Yang, F.; Murugan, R.; Wang, S.; Ramakrishna, S. Electrospinning of nano/micro scale poly(L-lactic acid) aligned fibers and their potential in neural tissue engineering. *Biomaterials* **2005**, *26*, 2603–2610. [[CrossRef](#)] [[PubMed](#)]
34. Jin, H. Human bone marrow stromal cell responses on electrospun silk fibroin mats. *Biomaterials* **2004**, *25*, 1039–1047. [[CrossRef](#)]
35. Li, W.J.; Tuli, R.; Huang, X.; Laquerriere, P.; Tuan, R.S. Multilineage differentiation of human mesenchymal stem cells in a three-dimensional nanofibrous scaffold. *Biomaterials* **2005**, *26*, 5158–5166. [[CrossRef](#)] [[PubMed](#)]
36. Dalby, M.J.; McCloy, D.; Robertson, M.; Agheli, H.; Sutherland, D.; Affrossman, S.; Oreffo, R.O. Osteoprogenitor response to semi-ordered and random nanotopographies. *Biomaterials* **2006**, *27*, 2980–2987. [[CrossRef](#)] [[PubMed](#)]
37. Silva, G.A.; Czeisler, C.; Niece, K.L.; Beniash, E.; Harrington, D.A.; Kessler, J.A.; Stupp, S.L. Selective Differentiation of Neural progenitor cells by high-epitope density nanofibers. *Science* **2004**, *303*, 1352–1355. [[CrossRef](#)] [[PubMed](#)]
38. Curtis, A.; Wilkinson, C. Nanotechniques and approaches in biotechnology. *Trends Biotechnol.* **2001**, *19*, 97–101. [[CrossRef](#)]
39. Mengsteab, P.Y.; Uto, K.; Smith, A.S.; Frankel, S.; Fisher, E.; Nawas, Z.; Macadangdang, J.; Ebara, M.; Kim, D.H. Spatiotemporal control of cardiac anisotropy using dynamic nanotopographic cues. *Biomaterials* **2016**, *86*, 1–10. [[CrossRef](#)] [[PubMed](#)]
40. Matsumoto, H.; Ishiguro, T.; Konosu, Y.; Minagawa, M.; Tanioka, A.; Richau, K.; Kratz, K.; Lendlein, A. Shape-memory properties of electrospun non-woven fabrics prepared from degradable polyesterurethanes containing poly(omega-pentadecalactone) hard segments. *Eur. Polym. J.* **2012**, *48*, 1866–1874. [[CrossRef](#)]
41. Fejos, M.; Molnar, K.; Karger-Kocsis, J. Epoxy/Polycaprolactone Systems with Triple-Shape Memory Effect: Electrospun Nanoweb with and without Graphene versus Co-Continuous Morphology. *Materials* **2013**, *6*, 4489–4504. [[CrossRef](#)] [[PubMed](#)]
42. Ji, F.; Zhu, Y.; Hu, J.; Liu, Y.; Yeung, L.; Ye, G. Smart polymer fibers with shape memory effect. *Smart Mater Struct.* **2006**, *15*, 1547–1554. [[CrossRef](#)]
43. Barmouz, M.; Behraves, A.H. Shape memory behaviors in cylindrical shell PLA/TPU-cellulose nanofiber bio-nanocomposites: Analytical and experimental assessment. *Compos. Part A* **2017**, *101*, 160–172. [[CrossRef](#)]
44. Kawaguchi, K.; Iijima, M.; Miyakawa, H.; Ohta, M.; Muguruma, T.; Endo, K.; Nakazawa, F.; Mizoguchi, I. Effects of chitosan fiber addition on the properties of polyurethane with thermo-responsive shape memory. *J. Biomed. Mater. Res. B Appl. Biomater.* **2017**, *105*, 1151–1156. [[CrossRef](#)] [[PubMed](#)]

45. Aslan, S.; Kaplan, S. Thermomechanical and Shape Memory Performances of Thermo-sensitive Polyurethane Fibers. *Fibers Polym.* **2018**, *19*, 272–280. [[CrossRef](#)]
46. Karger-Kocsis, J.; Keki, S. Biodegradable polyester-based shape memory polymers: Concepts of (supra)molecular architecturing. *Express Polym. Lett.* **2014**, *8*, 397–412. [[CrossRef](#)]
47. Lim, D.I.; Park, H.S.; Park, J.H.; Knowles, J.C.; Gong, M.S. Application of high-strength biodegradable polyurethanes containing different ratios of biobased isomannide and poly (-caprolactone) diol. *J. Bioact. Compat. Polym.* **2013**, *28*, 274–288. [[CrossRef](#)] [[PubMed](#)]
48. Maeda, T.; Kim, Y.J.; Aoyagi, T.; Ebara, M. The design of temperature-responsive nanofiber meshes for cell storage applications. *Fibers* **2017**, *5*, 13. [[CrossRef](#)]
49. Zhu, Y.; Hu, J.; Yeung, L.-Y.; Liu, Y.; Ji, F.; Yeung, K.-W. Development of shape memory polyurethane fiber with complete shape recoverability. *Smart Mater. Struct.* **2006**, *15*, 1385–1394. [[CrossRef](#)]
50. Ping, P.; Wang, W.; Chen, X.; Jing, X. Poly(e-caprolactone) polyurethane and its shape-memory property. *Biomacromolecules* **2004**, *6*, 587–592. [[CrossRef](#)] [[PubMed](#)]
51. Guan, J.-L. Role of focal adhesion kinase integrin Signaling. *Int. J. Biochem. Cell. Biol.* **1997**, *29*, 1085–1096. [[CrossRef](#)]
52. Li, F.; Hou, J.; Zhu, W.; Zhang, X.; Xu, M.; Luo, X.; Ma, D.; Kim, B.K. Crystallinity and morphology of Segmented Polyurethanes with Different Soft-Segment Length. *J. Appl. Polym. Sci.* **1996**, *62*, 631–638. [[CrossRef](#)]



© 2019 by the authors. Licensee MDPI, Basel, Switzerland. This article is an open access article distributed under the terms and conditions of the Creative Commons Attribution (CC BY) license (<http://creativecommons.org/licenses/by/4.0/>).